



Detecting nitrogen oxide emissions in Qatar and quantifying emission factors of gas-fired power plants – a 4-year study

Anthony Rey-Pommier^{1,2}, Frédéric Chevallier¹, Philippe Ciais^{1,2}, Jonilda Kushta²,
Theodoros Christoudias², I. Safak Bayram³, and Jean Sciare²

¹Laboratoire des Sciences du Climat et de l'Environnement, LSCE/IPSL, CEA-CNRS-UVSQ,
Université Paris-Saclay, 91198 Gif-sur-Yvette, France

²The Cyprus Institute, Climate and Atmosphere Research Center, 2121 Nicosia, Cyprus

³Department of Electronic and Electrical Engineering, University of Strathclyde,
Glasgow G1 1XW, United Kingdom

Correspondence: Anthony Rey-Pommier (anthony.rey-pommier@lscce.ipsl.fr)

Received: 16 May 2023 – Discussion started: 12 June 2023

Revised: 5 September 2023 – Accepted: 23 September 2023 – Published: 30 October 2023

Abstract. Nitrogen oxides ($\text{NO}_x = \text{NO} + \text{NO}_2$), produced in urban areas and industrial facilities (particularly in fossil-fuel-fired power plants), are major sources of air pollutants, with implications for human health, leading local and national authorities to estimate their emissions using inventories. In Qatar, these inventories are not regularly updated, while the country is experiencing fast economic growth. Here, we use spaceborne retrievals of nitrogen dioxide (NO_2) columns at high spatial resolution from the Tropospheric Monitoring Instrument (TROPOMI) to estimate NO_x emissions in Qatar from 2019 to 2022 with a flux-divergence scheme, according to which emissions are calculated as the sum of a transport term and a sink term representing the three-body reaction comprising NO_2 and hydroxyl radical (OH). Our results highlight emissions from gas power plants in the northeast of the country and from the urban area of the capital, Doha. The emissions from cement plants in the west and different industrial facilities in the southeast are underestimated due to frequent low-quality measurements of NO_2 columns in these areas. Our top-down model estimates a weekly cycle, with lower emissions on Fridays compared to the rest of the week, which is consistent with social norms in the country, and an annual cycle, with mean emissions of 9.56 kt per month for the 4-year period. These monthly emissions differ from the Copernicus Atmospheric Monitoring Service global anthropogenic emissions (CAMSGLOB-ANT_v5.3) and the Emissions Database for Global Atmospheric Research (EDGARv6.1) global inventories, for which the annual cycle is less marked and the average emissions are respectively 1.67 and 1.68 times higher. Our emission estimates are correlated with local electricity generation and allow us to infer a mean NO_x emission factor of $0.557 \text{ t}_{\text{NO}_x} \text{ GWh}^{-1}$ for the three gas power plants in the Ras Laffan area.

1 Introduction

Nitrogen oxides are reactive trace gases that can be converted into other chemical species, including ozone and fine particulate matter. Emissions of NO_x can originate from natural sources (from fires, lightning and soils), but the majority originate from anthropogenic sources, such as vehicle engines and heavy industrial facilities like power plants, steel

mills and cement kilns (van Vuuren et al., 2011). High levels of NO_x in the troposphere contribute to the formation of acid rain and smog. They also have a significant effect on human health by causing various respiratory diseases (Bovensmann et al., 1999; Burnett et al., 2004; U.S. EPA, 2016; He et al., 2020). To limit those impacts, national and regional governments generally enact a series of air pollution control

strategies, which generally take the form of proscriptions on certain polluting technologies, with the aim of reducing the concentration of pollutants at the local level to targets that must be reached within a given time frame. In the Middle East region, such mitigation strategies are quite recent. The region is thus experiencing increasing levels of NO_x pollution from anthropogenic sources (Osipov et al., 2022), with levels that remain high by international standards (Lelieveld et al., 2015). During the last 2 decades, Qatar experienced a rapid development based on oil and gas, leading to a degradation of air quality (Mansouri Daneshvar and Hussein Abadi, 2017). However, no official report concerning emissions of pollutants has been publicly available in the last 12 years.

Spectrally resolved satellite measurements of solar backscattered UV–visible radiation enable the quantification of NO₂ in the atmosphere. Such measurements have been providing information on the spatial distribution of tropospheric NO₂ for more than 20 years, allowing the identification of many NO_x sources globally (Richter and Burrows, 2002; Celarier et al., 2008). In October 2017, the Sentinel-5 Precursor satellite was launched. Its main instrument is the TROPOspheric Monitoring Instrument (TROPOMI), which provides daily tropospheric NO₂ column densities at high spatial resolution with a large swath width. Column images can then be used to retrieve NO_x emissions with the use of the continuity equation in a steady state. This scheme, known as flux divergence, requires the use of other physical quantities. In this study, we use this method to quantify the emissions in Qatar based on retrievals from 2019 to 2022 and to overcome the absence of recent reporting.

This article is organized as follows: Sect. 2 provides a description of Qatar and its main emission sources. Section 3 provides a description of the datasets used in this study. Section 4 presents the flux-divergence method to infer NO_x emissions at the scale of the country. Section 5 presents the spatial distribution of NO_x emissions and their seasonal variations. It also presents the limitation of our method in terms of inferring emissions for areas above which TROPOMI measurements are often of low quality. Section 6 compares our estimated emissions to local electricity generation and existing global inventories to provide a sectoral approach to NO_x emissions. Section 7 presents the limits and the uncertainties of the model, and Sect. 8 presents our concluding remarks. For the purposes of our study, NO_x emissions are expressed as NO₂ throughout this article.

2 General features of Qatar and overview of reported NO_x emissions in 2007

Qatar is a country with an area of 11 600 km², located on the northeast coast of the Arabian Peninsula. The country shares its sole terrestrial border with Saudi Arabia in the south and has maritime boundaries with Bahrain in the west, Iran in the north and the United Arab Emirates in the east. Qatar

has the third largest proven natural gas reserves in the world and non-negligible oil reserves (EIA, 2021). Since 1973, oil and gas revenues increased dramatically, making the country the third largest exporter of natural gas (OPEC, 2020). The resulting economic growth raised Qatar to being one of the countries with the highest per capita incomes in the world. Between 2001 and 2019, the average GDP growth rate of the country was 9.1 % (World Bank, 2022), driven by the exploitation of the oil and gas fields, which account for 85 % of its exports and over 60 % of its gross domestic product. The exploitation of such oil and gas resources is a source of air pollution due to NO_x emissions during the incomplete combustion of hydrocarbons. The power sector, which is dominated by gas power plants, and the transport sector are thus important contributors to the NO_x levels throughout the country. Other sectors, such as cement production, also contribute to the total NO_x budget. Little information is available on the country's emissions and the share of these different sectors. The last official communication dates back to 2011 for emissions in 2007 and uses the IPCC Common Reporting Format sector classification (Ministry of Environment, Qatar, 2011). It estimates total emissions of 163 kt (assumed to be expressed as NO₂), with the following shares:

Power generation. There are several gas-fired power plants in Qatar which, until the end of 2022, provided all the electricity in the country, with a generation that increased from 4.5 TWh in 1990 to 48 TWh in 2021 (EIA, 2022). According to the report for emissions in 2007, they produced 32.03 kt of NO_x, which corresponded to 19.7 % of the country's total emissions. The report indicates an emission factor equal to 0.109 t_{NO_x} TJ⁻¹ or 0.392 t_{NO_x} GWh⁻¹, which is a low but realistic emission factor for an electric mix dominated by gas. More recent data on NO_x emissions from the power sector are not available.

Cement production. The country has three cement production sites. According to the report for emissions in 2007, cement production was responsible for 23.4 % of the country's total NO_x emissions. It should be noted that, due to the high temperatures in summer, outdoor activities at the production sites are reduced, which can result in lower activity between June and September.

Road transport. According to the report for emissions in 2007, the road transport sector accounted for 22.7 % of the country's total NO_x emissions (27.6 % for the total transport sector). Fuel sales do not seem to have any annual seasonality (Al-Attiyah Foundation, 2018); the corresponding NO_x emissions are therefore not variable with the seasons. However, they may change gradually with the nature of the vehicle fleet, which includes a growing number of diesel vehicles.

Manufacture of solid fuels and other energy industries. This sector includes upstream oil and gas activities and

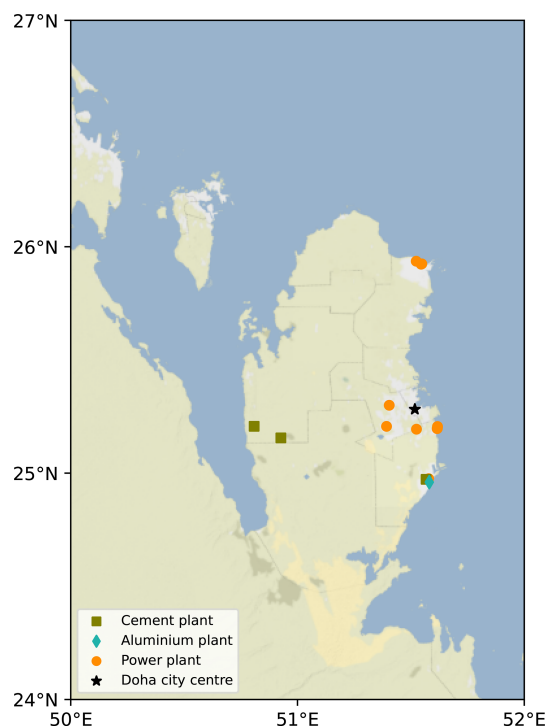


Figure 1. Location of the main industrial facilities (cement kilns, power plants and aluminium smelters) in Qatar. Urban areas are displayed in grey, and Doha's city centre is denoted with a star. Industrial facilities and cities in other countries are not displayed. Map tiles by Stamen Design under CC BY 3.0. Data from © OpenStreetMap contributors.

processing operations. Most of the historical upstream operations took place in the Dukhan Field, located in the west of the country, but the majority of the extraction currently takes place offshore in the North Field, which is one of the largest non-associated gas fields in the world. According to the report for emissions in 2007, these activities accounted for 25.7 % of the country's NO_x emissions.

Figure 1 shows the locations of the industrial facilities in Qatar which are likely to emit significant amounts of NO_x. Four regions can be distinguished. The west of the country comprises two large-capacity cement plants (7.0 and 5.0 Mt yr⁻¹). The southeast includes a gas power plant, a cement plant and an aluminium smelter, while the northeast comprises the industrial area of Ras Laffan, including three gas power plants. Finally, the urban area of Doha, in the central eastern part of the country, contains the majority of the population, as well as five gas power plants.

3 Instruments and data

3.1 TROPOMI NO₂ retrievals

NO₂ can be observed from space with satellite instruments based on its strong absorption features in the 400–465 nm wavelength region (Vandaele et al., 1998). By comparing observed spectra with a reference spectrum, the amount of NO₂ in a portion of the atmosphere between the instrument and the surface can be derived. The TROPOspheric Monitoring Instrument (TROPOMI), on board the European Space Agency's (ESA) Sentinel-5 Precursor (S-5P) satellite, is one of those instruments, providing daily measurements of NO₂ around 13:30 local time (LT; the time zone for all instances in the text is LT). Its high spatial resolution (originally 3.5 × 7 km² at nadir, improved to 3.5 × 5.5 km² since 6 August 2019) allows one to observe some of the fine-scale structures of NO₂ pollution, such as within cities (Beirle et al., 2019; Demetillo et al., 2020) or near power plants and industrial facilities (Shikwambana et al., 2020; Saw et al., 2021). Tropospheric vertical column densities (VCDs or simply columns) are provided by the algorithm after measurement by the instrument, which represents the vertically integrated number of NO₂ molecules per surface unit between the surface and the tropopause. An algorithm also provides an air mass factor (AMF), which is used to convert slant column densities into vertical column densities. This factor depends on many parameters, including the albedo of the viewed surface, the vertical distribution of the absorber and the viewing geometry. It is a source of structural uncertainty in NO₂ measurements (Boersma et al., 2004; Lorente et al., 2019), which becomes non-negligible in polluted environments. The large swath width of the instrument (~ 2600 km) makes it possible to construct NO₂ images of VCDs on large spatial scales. We use TROPOMI NO₂ retrievals from 2019 to 2022 (S5P-PAL reprocessed data with processor version 2.3.1 from January 2019 to October 2021, offline (OFFL) stream with processor version 2.3.1 from November 2021 to October 2022 and OFFL stream with processor version 2.4.0 from November to December 2022) over Qatar. The arid climate of the country, which offers a large number of clear-sky days throughout the year, enables the calculation of monthly averages based on multiple observations. Its intensive anthropogenic activity, concentrated on a small number of areas, allows one to observe high NO₂ concentration patterns. Due to its short lifetime (about 1 to 10 h), background NO₂ levels can be orders of magnitude lower than levels near polluted areas. Pollution patterns are therefore characterized by large signal-to-noise ratios above main emitters. Finally, TROPOMI products provide a quality assurance value q_a , which ranges from 0 (no data) to 1 (high-quality data). For our analysis of concentrations, we selected NO₂ retrievals with q_a values greater than 0.75, which systematically correspond to clear-sky conditions (Eskes et al., 2022), and gridded these retrievals at a spatial resolution of 0.0625° × 0.0625°. From August 2019,

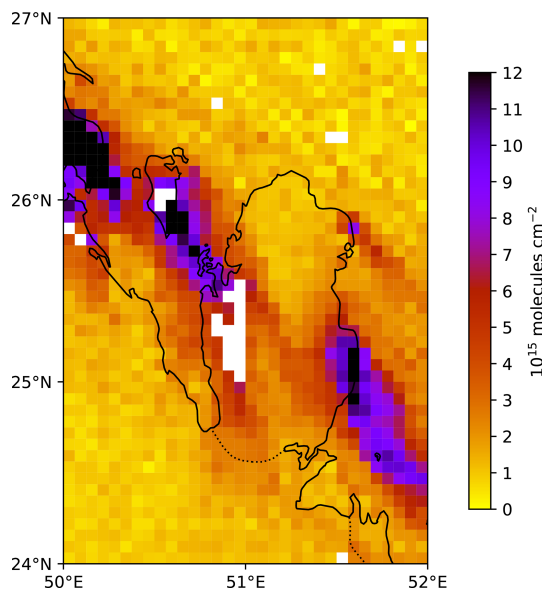


Figure 2. TROPOMI observation of NO₂ column densities above Qatar on 12 December 2019. White pixels correspond to areas with low-quality data ($q_a < 0.75$) or no data.

this resolution is lower than that of the instrument, thus providing a grid for which NO₂ VCDs correspond to one or more measurements. The observed plumes remain correctly resolved.

The domain of interest extends between the parallels of 24 and 27° N and the meridians of 50 and 52° E. TROPOMI tropospheric columns show polluted areas, such as the Ras Laffan area, but also the large urban area of Doha. Observed VCDs are high (5 to 30×10^{15} molec. cm⁻²), which facilitates the observation of NO₂ plumes. An example of a TROPOMI image is provided in Fig. 2. Within the domain, the meridional component of the wind is generally oriented towards the south. The zonal component varies throughout the year. Strong wind events can cause the pollution from Bahrain to reach the coasts of Qatar. Finally, several areas in the west of the country are not visible by TROPOMI most of the time because the quality of the corresponding measurements is too low. This phenomenon, which is also present in the east of the country (slightly south of downtown Doha) but with a smaller spatial extent, is studied in detail in Sect. 5.3.

3.2 ERA5

The horizontal wind vector field $\mathbf{w} = (u, v)$ is taken from the European Centre for Medium-Range Weather Forecasts (ECMWF) ERA5 data archive (fifth generation of atmospheric reanalyses) at a horizontal resolution of $0.25^\circ \times 0.25^\circ$ on 37 pressure levels (Hersbach et al., 2020). The hourly values have been linearly interpolated to the TROPOMI orbit timestamp and re-gridded to a $0.0625^\circ \times 0.0625^\circ$ resolution.

3.3 CAMS real-time fields

The Copernicus Atmospheric Monitoring Service (CAMS) global near-real-time service provides analyses and forecasts for reactive gases, greenhouse gases and aerosols. Data are gridded on 25 vertical pressure levels with a horizontal resolution of $0.4^\circ \times 0.4^\circ$ and a temporal resolution of 3 h (Huijnen et al., 2019). Here, CAMS concentration fields of hydroxyl radical (OH) are used to calculate NO₂ sinks from TROPOMI observations. We also use CAMS temperature field T to account for the reaction rate for HNO₃ production through the calculation of the NO₂ lifetime according to Burkholder et al. (2020). The hourly values are also linearly interpolated to the TROPOMI orbit timestamp and re-gridded to a $0.0625^\circ \times 0.0625^\circ$ resolution.

3.4 Inventories

The Emissions Database for Global Atmospheric Research (EDGARv6.1) and the CAMS global anthropogenic emissions (CAMS-GLOB-ANT_v5.3) are global inventories that provide $0.1^\circ \times 0.1^\circ$ gridded emissions for different sectors on a monthly basis. EDGARv6.1 emissions are based on activity data (population, energy production, fossil fuel extraction, industrial processes, agricultural statistics, etc.) derived from the International Energy Agency (IEA) and the Food and Agriculture Organization (FAO), corresponding emission factors, national and regional information on technology mix data, and end-of-pipe measurements. The inventory covers the years 1970–2018. CAMS-GLOB-ANT_v5.3 is developed within the framework of the Copernicus Atmospheric Monitoring Service (Granier et al., 2019). For this inventory, NO_x emissions are based on various sectors in the EDGARv5.0 emissions up to 2015, which are extrapolated to 2021 using sectorial trends from the Community Emissions Data System (CEDS) inventory (Hoesly et al., 2018) up to 2019. From one inventory to another, the names and definitions of the sectors may differ. In EDGARv6.1 and CAMS-GLOB-ANT_v5.3, the emissions for a given country are derived from the type of technologies used, the dependence of emission factors on fuel type, combustion conditions, and activity data and low-resolution emission factors (Janssens-Maenhout et al., 2019).

3.5 Electricity consumption and production data

As the power sector is one of the main drivers of NO_x, we use electricity production and consumption data at several timescales, as detailed in Sect. 5.5. Daily load profiles from February 2016 to January 2017 are taken from Bayram et al. (2018) and used to calculate monthly ratios between the average power demand and the power demand during the overpass of TROPOMI. These ratios are assumed to be valid from 2019 to 2022. We also use monthly electricity generation time series from 2019 to 2022, which are provided

by the Qatar Ministry of Development Planning and Statistics (PSA, 2023). From 2019 to 2021, these time series can be completed with monthly reports from Kahramaa, which transmits and distributes the electricity generated by each of the country's power plants with great accuracy (Kahramaa, 2023). The corresponding data for 2022 are not available yet.

4 Method

4.1 Mask and background removal

In satellite retrievals, the NO₂ signal from a sparsely populated area or a small industrial facility may be difficult to identify due to high noise levels or natural emissions. As a consequence, detecting traces of non-natural emissions in TROPOMI NO₂ images is not a straightforward process. In the absence of anthropogenic sources, the NO₂ columns that are observed constitute a tropospheric background that varies between 0.2 and 1.0×10^{15} molec. cm⁻². At the global scale, this background is mostly due to soil emissions in the lower troposphere (Yienger and Levy, 1995; Hoelzemann et al., 2004). In the upper troposphere, NO₂ sources include lightning, convective injection and downwelling from the stratosphere (Ehhalt et al., 1992), but the factors controlling the resulting concentrations are poorly understood. According to state-of-art estimates, anthropogenic NO_x accounts for most of the emissions at the global scale, whereas natural emissions from fires, soils and lightning are smaller (Jaeglé et al., 2005; Müller and Stavrakou, 2005; Lin, 2012). In Qatar, the desert climate limits lightning and fire, and the share of the corresponding emissions within the background is thus expected to be low. As a first step, we estimate this background by excluding the part of the domain which is outside the territory of Qatar, as well as other regions with human activity, which include Bahrain and the neighbouring part of Saudi Arabia. The remaining pixels constitute an external mask within which we calculate the 5th percentile of the TROPOMI columns. The corresponding value is defined as the tropospheric background. Figure 3 displays the external mask, as well as an internal mask that gathers only pixels above Qatar's territory. This external mask is used in Sects. 5 and 6.

4.2 Flux-divergence method

As a second step, we derive top-down NO₂ production maps with the flux-divergence method, which was originally proposed by Beirle et al. (2019). It consists of applying the continuity equation in a steady state as follows:

$$e_{\text{NO}_2} = \text{div}(\Omega_{\text{NO}_2} \mathbf{w}) + \Omega_{\text{NO}_2} / \tau. \quad (1)$$

The previous equation highlights a transport term $D = \text{div}(\Omega_{\text{NO}_2} \mathbf{w})$, obtained by multiplying NO₂ VCDs with horizontal wind speeds and the NO₂ sinks $S = \Omega_{\text{NO}_2} / \tau$. As the local overpass time of TROPOMI is close to 13:30, sinks are

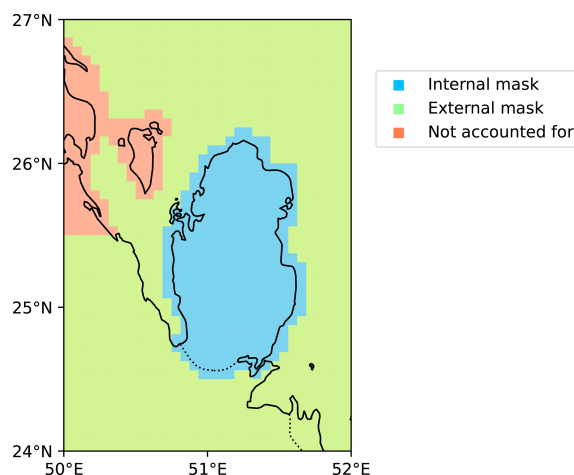


Figure 3. Masks used for NO_x emission estimates. Green cells are used to estimate the NO₂ tropospheric background that is removed from vertical column densities before calculation of emissions (external mask). Blue cells are used to count NO_x emissions attributable to Qatar (internal mask). Orange cells, which cover urban and industrial areas from other countries, are not considered.

dominated by the chemical loss due to the reactions of NO₂ with OH (leading to the formation of HNO₃), which can be described by the chemical lifetime τ as follows:

$$\tau = \frac{1}{k_{\text{mean}}(T, [M]) \cdot [\text{OH}]}. \quad (2)$$

Here, k_{mean} is the kinetic reaction rate that characterizes the different first-order reactions between NO₂ and OH. Burkholder et al. (2020) provide a general expression of this reaction rate with respect to atmospheric conditions (temperature T and total air concentration $[M]$).

In the atmosphere, OH is a dominant oxidant species. It is mainly produced during daylight hours by the interaction between water and atomic oxygen produced by ozone dissociation (Levy, 1971), and its concentration is therefore strongly correlated with solar ultraviolet radiation (Rohrer and Berresheim, 2006). The direct measurement of OH is possible using spectroscopic methods, but the spatial representativeness of the data is limited due to its short lifetime. Most global analyses thus estimate OH budgets from other variable species (Li et al., 2018; Wolfe et al., 2019) with high associated uncertainties (Huijnen et al., 2019). In polluted air, another mechanism for OH production is the reaction between NO and HO₂. This reaction, referred to as the NO_x recycling mechanism, illustrates the nonlinear dependence of the OH concentration on NO₂ (Valin et al., 2011; Lelieveld et al., 2016). Here, considering OH to be the only sink assumes that other sinks are negligible. We consider such an approximation to be valid (Rey-Pommier et al., 2022). This hypothesis can be validated a posteriori by analysing the calculated NO_x emission maps and verifying the absence of highly negative emissions (which would correspond, all other things

being equal, to an underestimation of the sink term) or emissions having the shape of a plume (which would correspond, all other things being equal, to an overestimation of the sink term).

Finally, it should be noted that anthropogenic combustion activities produce mainly NO, which is transformed into NO₂ by reaction with ozone O₃. NO₂ is then photolysed during the day, reforming NO (Seinfeld, 1989). This photochemical equilibrium between NO and NO₂ can be highlighted with the concentration ratio $L = [\text{NO}_x]/[\text{NO}_2]$. NO_x emissions are therefore obtained by multiplying NO₂ production e_{NO_2} by L . As diurnal NO concentrations in urban areas are generally above 20 ppb, the characteristic stabilization time of this ratio never exceeds a few minutes (Graedel et al., 1976; Seinfeld and Pandis, 2006). This time being lower than the order of magnitude of the inter-mesh transport time (about 30 min considering the resolution used and the mean wind module in the region), we can reasonably neglect the effect of the stabilization time of the conversion factor on the total composition of the emissions and treat each cell of the grid independently from its direct environment. In Rey-Pommier et al. (2022), this ratio was estimated using the CAMS NO and NO₂ concentration fields in Egypt. For Qatar, CAMS data show many outliers for these concentration fields: for some pixels, NO concentrations can be equal to zero. They can be also 2 times higher than NO₂ concentrations in places without any significant feature that would explain it. We therefore do not use these fields and choose a fixed value of 1.32 for this ratio, as used by Beirle et al. (2019). After removal of outliers in the statistics, CAMS values for L suggest that the average value for this ratio ranges between 1.17 and 1.60 with small spatial variations.

Through the OH concentration, we enable a variability in the chemical lifetime. This variability is not allowed in the original version of the first-divergence method by Beirle et al. (2019), which relied on heavy averaging over time to infer emissions at the scale of cities and power plants. Here, seasonal and spatial variations of lifetimes are resolved, thus limiting the errors in the estimation of the daily sink term. Although errors remain high when estimating daily emissions, averaged monthly emissions are correctly resolved above the main emitters.

5 Results

5.1 Selection of TROPOMI images and averages

We apply Eq. (1) to daily TROPOMI images and average the resulting emissions to obtain monthly daytime emissions. This process can be hindered due to the presence of poor-quality measurements that prevent the calculation of the divergence in the transport term each day. This happens when a significant part of the country is covered by clouds. Furthermore, the resolution used to grid data ($0.0625^\circ \times 0.0625^\circ$, i.e. about $6.3 \times 6.9 \text{ km}^2$ in this region) is lower than the initial res-

olution of TROPOMI ($3.5 \times 7 \text{ km}^2$ until 6 August 2019). For the first 8 months of this study, our gridding therefore results in maps having many pixels without data. In the process of estimating mean monthly emissions, we consider these two situations and do not take into account the averaging of the days for which corresponding TROPOMI images cover more than 70 % of the territory of Qatar (defined by the internal mask) without data or with poor quality data ($q_a < 0.75$). Furthermore, Bahrain is located 30 km away from Qatar, and the centres of the capitals of the two countries are separated by about 130 km. Pollution from Bahrain, which is usually transported to Qatar, can reach Doha during strong wind events. In such situations, the errors in ERA5 can alter the estimation of the transport term and thus the NO_x estimates. As a consequence, we also remove days with high wind speeds in the Bahrain–Qatar direction, i.e. days for which the average wind over Bahrain and the marine area between the two countries has a speed higher than 30 km h^{-1} and an angle between -15° (E1/4SE) and -75° (S1/4SE). The choice of these thresholds is discussed in the Supplement. Figure 4 shows the amount of days considered in the calculation of the average emissions of a given month between 2019 and 2022. It also shows the number of days that have been discarded and the reasons for the corresponding discards.

Here, monthly average emissions are calculated with between 8 and 25 d of TROPOMI images, with low values for the first 7 months of the study due to the lower resolution of TROPOMI during this period. Excluding these months, averages are calculated with 17.9 d. Cases for which too many pixels are not observed by TROPOMI in the internal mask occur more frequently than cases with strong winds from Bahrain. Overall, we consider most of the inferred monthly averages to be robust. However, at the small scale, there are a small number of pixels with a constant absence of reliable VCD estimations due to low-quality measurements, resulting with pixels having estimations of NO_x with a poor reliability. The treatment of such pixels is shown in Sect. 5.3.

5.2 Spatial distribution of NO_x emissions

We use the flux-divergence model to obtain NO_x emission maps within our domain. For each applicable day (as described in Sect. 5.1), a background is calculated using the external mask, and daily emissions are estimated. These daily emissions are then averaged to obtain a representation of the emissions at 13:30 on a monthly scale. For October 2022, a maximum of 25 daily emissions have been average to calculate the corresponding mean monthly emissions map, which is displayed in Fig. 5. When the transport term is integrated over large spatial scales, it cancels out due to the mass balance in the continuity equation between NO₂ sources and NO₂ sinks. Although the sink term is responsible for most of the total NO_x budget within the domain, the transport term can reach high values at a small scale, highlighting hotspots where emissions are concentrated. Such hotspots comprise

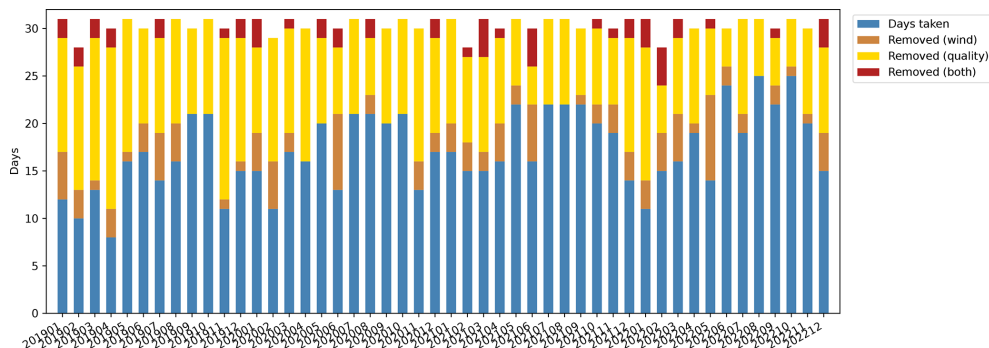


Figure 4. Number of days involved in the mean monthly estimates of NO_x emissions (blue) and days that have been discarded due to strong winds blowing from Bahrain to the southeast (brown), large areas within the internal mask with low-quality data (yellow) or both (red).

gas power plants in the northeastern part of the country and industrial facilities in the southeast. High emissions are also observed in Doha, but in that case, the sink term accounts for most of the NO_x budget due to the spread of sources in the urban area. The western part of the country, where two cement plants are located, also shows significant emissions. High emissions outside of Qatar are observed in the urban areas of Manama (Bahrain) and Dammam (Saudi Arabia). In the southeastern corner of the domain, an area of high emissions also seems to stand out from the desert. This area corresponds to a cross-border centre between Saudi Arabia and the United Arab Emirates. It is possible that important road traffic there is responsible for such emissions, but we have no information to support this hypothesis. Finally, we observe high emissions at sea, up to about 30 km from the eastern coast of the country. These emissions of about 2.0×10^{15} molec. cm⁻² h⁻¹ cannot be solely attributed to shipping activity (Rey-Pommier et al., 2022). Because in this region, the centre of the 40 km × 44 km CAMS pixel is close to the coast, the NO₂ lifetime is probably underestimated. The rest of the domain has relatively low emissions, which is consistent with the absence of major sources of NO_x.

Nevertheless, it can be noted that inferred emissions in the domain remain relatively noisy. From monthly maps, we calculate average emissions at 13:30 for the period 2019–2022, which are displayed in Fig. 6. The hotspots identified earlier remain visible with a improved signal-to-noise ratio. In particular, emissions in the northeastern region are superior to 3.0×10^{15} molec. cm⁻² for only seven pixels, which are among the pixels closest to the power plants in the region. In the eastern part of the country, NO_x emissions reflect the main directions of urban expansion in Doha (from the coast towards the west and the southwest), with emissions ranging from 2×10^{15} to 10×10^{15} molec. cm⁻² h⁻¹. The desert areas display very low emissions (about 0.2×10^{15} molec. cm⁻² h⁻¹), indicating a slight overestimation of the average sink term or an underestimation of the NO₂ background. Emissions at sea remain abnormally high on the east

coast, but the effect is lower than what is observed in Fig. 5. However, unlike for October 2022, for which the emissions from cement plants could be identified, we observe low emissions in the western part of the country.

5.3 Availability of TROPOMI data above industrial sites

High-quality measurements by TROPOMI are infrequent above the western and southeastern parts of Qatar, with pixels regularly corresponding to measurements with $q_a < 0.75$. For these pixels, the inferred emissions are only calculated with an average over a very small number of measurements. In many cases, no measurements are available, and emissions cannot be attributed to the pixels. Figure 7 shows the mean TROPOMI coverage over the domain for the year 2020, counted as fraction of days with $q_a < 0.75$ within the year. In addition to the west and southeast (corresponding to the southern part of Doha) already identified, the northeast is also affected but to a lesser extent. This situation is the same for the years 2019 and 2021, and the identified areas have a fraction of observable days lower than 40%. The situation is different for the year 2022, during which the west had a fraction of about 70% and the southeast had a fraction of about 50% (see the Supplement). The effect on the total inferred emissions is not negligible since pixels that are concerned include intensive emitters, such as an industrial area in the southeast and the two large cement plants in the west. For instance, during the 36 months of the period 2019–2021, inferred emissions above these cement plants were lower than 1.5×10^{15} molec. cm⁻² h⁻¹ for 8 months and greater than this value for 8 months. Emissions could not be inferred for at least one of the plants for the remaining 20 months. Conversely, emissions could be inferred for 10 months out of 12 in 2022, and they were higher than 1.5×10^{15} molec. cm⁻² h⁻¹ for 6 of those months. In the TROPOMI products, the value of q_a includes automated quality assurance parameters related to different algorithms concerning the presence of clouds, aerosol particles, pressure levels and other physical quantities. For situations with

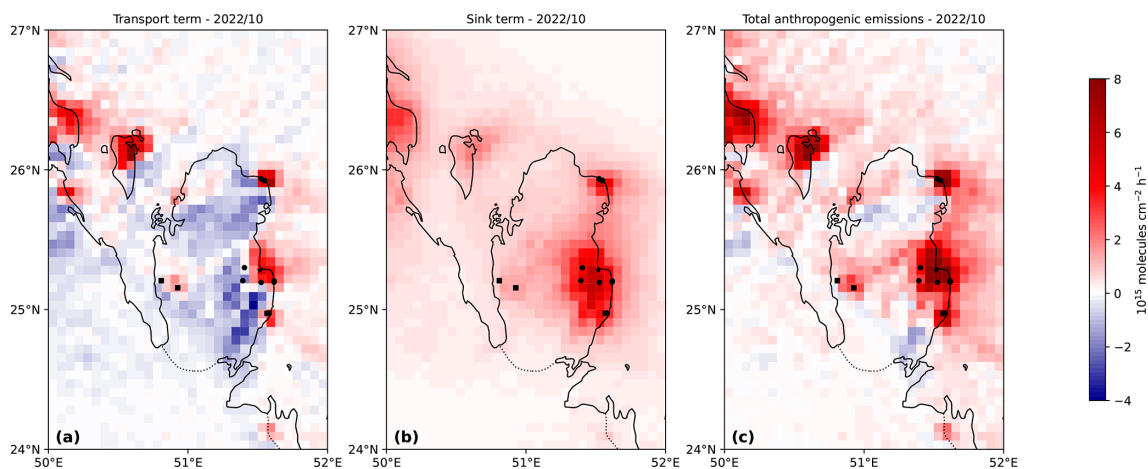


Figure 5. Mean NO_x emissions above Qatar (13:30): transport term (a), sink term (b) and resulting emissions (c) for October 2022. Power plants are denoted with dots, cement plants are denoted with squares, and Doha's city centre is denoted with a star.

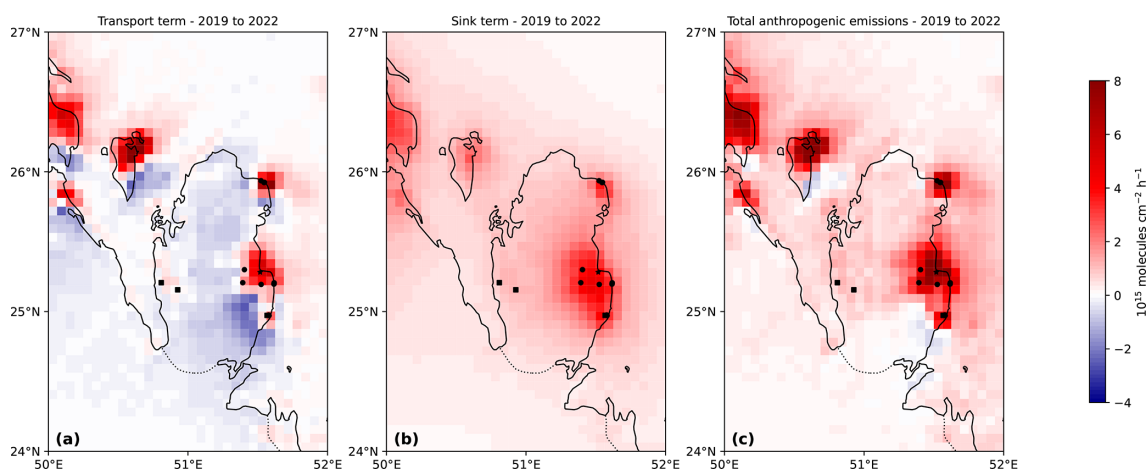


Figure 6. Mean NO_x emissions above Qatar (13:30): transport term (a), sink term (b) and resulting emissions (c) for the 2019–2022 period. Power plants are denoted with dots, cement plants are denoted with squares, and Doha's city centre is denoted with a star.

$q_a < 0.75$, retrievals are only sensitive to the NO₂ concentrations above the clouds and will depend on model assumptions for the missing part. They still contain useful information, but this information should be carefully interpreted. Here, all areas that are affected by these low values are located near the coasts. These areas are not characterized by persistent clouds, but they are all located within or close to urban or industrial centres, in which aerosol emissions can be high. However, other regions in Qatar and the neighbouring countries are characterized by high emissions of aerosols without q_a values being particularly high there. For instance, many studies have been providing estimates of NO_x emissions in Riyadh (Beirle et al., 2019) without indicating anything similar. We observe that these high frequencies of low q_a values are found in several urban and industrial areas on both coasts of the Persian Gulf (especially in Saudi Arabia, the United Arab Emirates and Iran). This suggests that the iden-

tified persistent low values for q_a come from the calculation of one or several quality assurance parameters. Because the areas displaying low values usually have a rectangular shape, it also suggests a low resolution for these parameters.

Here, we observe that the use of the OFFL stream (version 2.3.1) from November 2021 to October 2022 generates fewer pixels for which the value of q_a falls below 0.75 compared to the use of the S5P-PAL data from January 2019 to October 2021. Furthermore, the last 2 months of 2022, calculated with the version 2.4.0 of the NO₂ product (operational since July 2022), do not show any area with particularly low-quality flag values (see the Supplement). The latest version of the user manual indicates that, in this last version, the surface albedo climatology (SAC) used in the NO₂ fitting window and derived from OMI and GOME-2 was replaced by a SAC derived from TROPOMI observations (Eskes et al., 2022). This new TROPOMI SAC is consistently applied

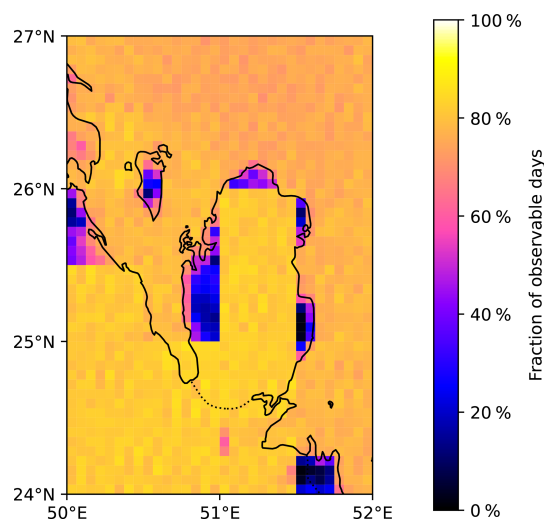


Figure 7. TROPOMI observation density for 2020.

in the cloud fraction, in the cloud pressure retrievals and in the air mass factor calculation. In the low- q_a areas identified in Fig. 7, it is therefore possible that high levels of aerosol-generating industrial activities in a small number of pixels in the grid results in a value of q_a below 0.75 in those pixels but also in all the surrounding pixels due to the low resolution of the parameter responsible for exceeding the threshold without these pixels being located over particularly emissive zones. This effect would be absent in the version 2.4.0 of the TROPOMI product. For the first 34 months of our study, the calculated monthly emissions for these areas would be then underestimated because they would correspond to the days with low industrial activity.

To evaluate the impact of this effect, we apply the same model using a threshold value of q_a corresponding to 0.7. This includes many pixels that would be rejected with a threshold of 0.75. As the TROPOMI manual recommends not using this threshold level, we do not consider these emissions to be representative of human activity in Qatar, and they are not treated as emissions estimates. Nevertheless, it allows us to evaluate the effect of non-detection of cement plants and power plants in the southeast of the domain. The use of a threshold value of $q_a = 0.7$ increases the inferred fluxes by 43.8% above cement plants in the west and by 33.4% above the industrial area in the southeast. Fluxes for the Ras Laffan area in the north and central Doha, which are less affected by the effect described here, are increased by 2.6% and 3.0% respectively. It is difficult to determine whether these increases are realistic because they were obtained using columns where NO₂ might have been estimated above aerosol and cloud layers. However, they indicate that our model, run with TROPOMI data before November 2021, leads to a systematic underestimation of NO_x emissions in two of the four most NO_x-intensive areas of the country. We note, however, that, on average, these increases are compen-

sated for: with a threshold of $q_a = 0.7$, total fluxes within the internal mask are reduced by 2.1% because fluxes outside the main emissive areas, which comprise most of the mask, are reduced by about 17%.

5.4 Weekly cycle

In Qatar, the official rest day is Friday, and the economic activity of the country is lower during this day than during the other days of the week. We therefore try to characterize this feature by evaluating the weekly cycle of NO_x emissions. We use the TROPOMI-inferred emissions to obtain averages per day of the week. We use the flux-divergence method to calculate the emissions within the internal mask. We remove the days for which most of the area contains poor-quality measurements and those for which the wind from Bahrain blows to the southeast. This is the same way the method was conducted in Sect. 5.1.

For a given day, the empty pixels (i.e. those to which it was not possible to assign emissions) are filled with the average of the emissions obtained for the remaining pixels. This choice leads to an underestimation of the emissions when the main emitting areas are covered by clouds or aerosols and to an overestimation in the opposite case. To limit this effect, we remove from our estimate of annual averages the emissions below the 5th percentile and above the 95th percentile. Figure 8 shows the resulting daily emissions for the 4-year period. Each year, a Friday minimum is observed, defining a weekly cycle. This trend is also observed for mean NO₂ column densities but not for OH concentrations. It is also more pronounced for residential areas, for which the Friday activity is 40% lower than the weekly average. Conversely, the effect is weaker above the power plants in the north of the country, which are located more than 30 km away from major residential areas (see the Supplement). At the scale of the country, Fridays have average emissions of 9.04 t h⁻¹, which is lower than average emissions for the rest of the week, which reach 14.15 t h⁻¹. In Middle-Eastern countries, this “week-end” effect had already been inferred from satellite measurements by Stavrakou et al. (2020) and Rey-Pommier et al. (2022) and from ground measurements by Butenhoff et al. (2015) on NO₂ concentrations but with a lower difference between Fridays and the other days.

5.5 Scaling of emissions and annual cycle

In this study, we estimate the emissions at around 13:30, which corresponds to the moment when TROPOMI overpasses the country. However, anthropogenic activity is not uniform throughout the day, and the emissions inferred from parameters calculated at 13:30 do not correspond to the average emissions of the country. Using the power consumption data from Bayram et al. (2018), Fig. 9 shows the mean load curve for the country on April 2016, July 2016, October 2016 and January 2017. These curves show that the average

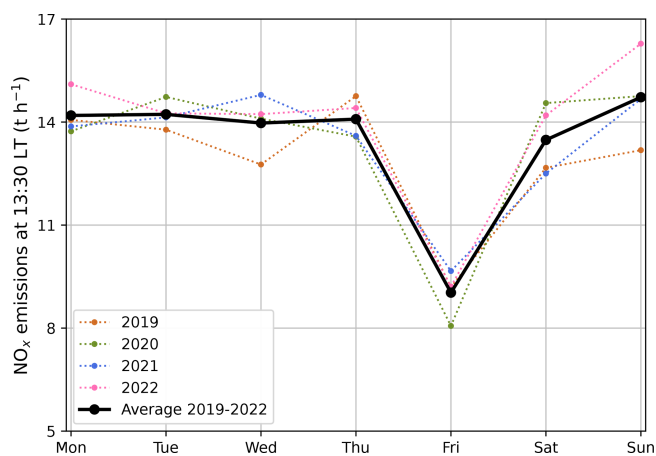


Figure 8. Mean weekly profiles of anthropogenic NO_x emissions at 13:30 in Qatar using TROPOMI observations for 2019 to 2022. The average emissions for the 4-year period are displayed with the black line.

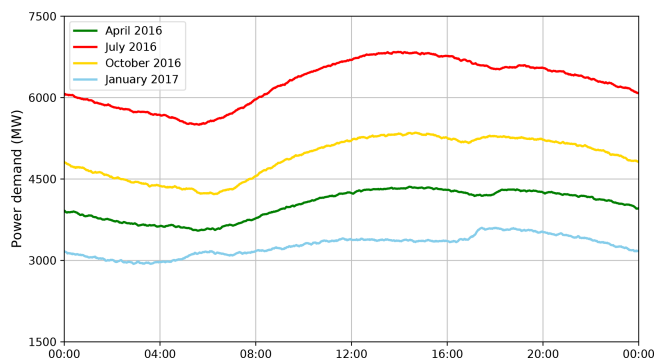


Figure 9. Monthly mean power demand in Qatar for 4 different months in 2016–2017.

power injected into the grid is slightly lower than the power injected at 13:30. The ratio between the two powers is minimal in June, where it reaches 0.911, and maximal in February, where it reaches 0.976 (see the Supplement). Moreover, according to the traffic congestion index in Doha (Tomtom, 2023), the road traffic around 13:30 shows a congestion peak that is slightly lower than the other peaks that occur at the beginning and the end of the daytime. This suggests that the average emissions from the road transport sector are also close to those at 13:30, with a similar ratio to that of the power sector.

We therefore re-scale the inferred NO_x emissions at the scale of the country by multiplying the monthly estimate for 13:30 with the power ratio to estimate mean monthly emissions. We acknowledge that this is a simplification: the power sector has a variable emission factor due to the different technologies in the power plants that are used to respond to the electricity demand over the year, and the road congestion level does not necessarily reflect traffic emissions. Moreover,

other sectors, such as cement production, whose seasonality is unknown to us, might behave differently.

Within the internal mask, Fig. 10 shows total NO_x emissions in Qatar using our method. Since the NO₂ background has been removed from VCD calculations, the total NO_x budget calculated for each month corresponds to the NO_x production by human activities. The annual variability is marked, with higher emissions in summer and lower emissions in winter. On average, NO_x emissions reach 9.56 kt per month. With mean emissions of 9.29 and 10.08 kt, 2019 and 2022 appear to be the years with lowest and highest mean emissions respectively. No seasonal cycle seems to appear for VCDs, except above the greater Doha area, which undergoes NO₂ levels that are about 23 % higher than the 2019–2022 average from October to January, while they are 27 % lower from June to August. To obtain the observed cycle in NO_x emissions, these differences in VCDs over Doha suggest a more intense oxidation in summer, which is captured by higher OH values for summer months. This is consistent with nonlinear effects in the NO₂ loss rate, with an absolute growth rate that is higher for OH than for NO₂ VCDs at high NO₂ levels inside the plume (Valin et al., 2011). However, because wind speeds tend to be higher during summer in Qatar, the observed variations in VCDs over Doha can also be partially explained by a spread of the pollution beyond the shores of the country. The uncertainties, detailed in Sect. 7, are higher for the months for which emissions could not be attributed for the western and southeastern parts of the territory. This hinders year-on-year comparisons. Consequently, although emissions in the March–April–May (MAM) 2020 period are 96 % and 87 % of the level of emissions in MAM 2019 and MAM 2021 respectively, we cannot assert whether this effect can be attributed to the restrictions put in place from March to May 2020 to tackle the Covid-19 pandemic. This caution is all the more necessary as these restrictions have been less stringent than in other countries (Hale et al., 2021). Similarly, higher emissions during 2022 could be due to the different values reached by q_a in the 2.4.0 version of the TROPOMI product with respect to the 2.3.1 version. However, it cannot be excluded that these higher emissions were due to a more intense activity in 2022 in the context of organizing the FIFA World Cup.

6 Comparison with air pollution inventories and electricity generation data

As Qatar is a small country with an undiversified economy, the annual cycle of the TROPOMI-inferred emissions can be interpreted. Reported emissions reached 163 kt in 2007, but a significant part did not take place within the terrestrial borders of the country. To compare such reported emissions with those calculated within the internal mask, emissions from upstream oil and gas operations (41.86 kt), which mostly take place offshore, must be removed from the pre-

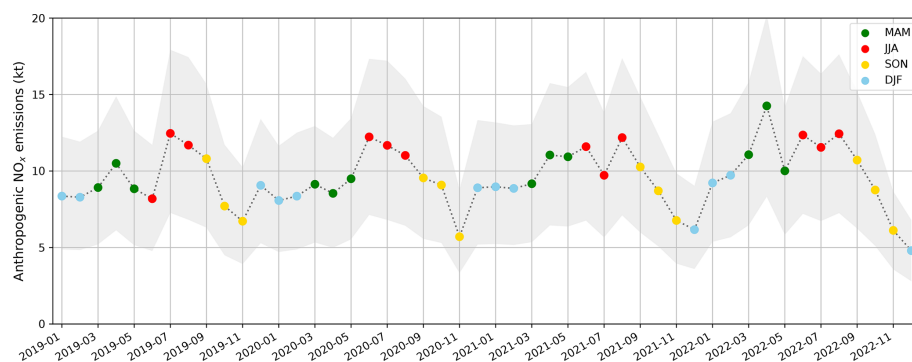


Figure 10. Total TROPOMI-derived anthropogenic NO_x emissions in Qatar from 2019 to 2022 using the flux-divergence method. The colours are used to illustrate seasonal variations (green: MAM; red: JJA; yellow: SON; blue: DJF).

vious budget. We also remove emissions from navigation (4.35 kt), civil aviation (3 kt) and fugitive emissions (4.28 kt). Reported terrestrial emissions therefore reach the approximate value of 109.51 kt for 2007, i.e. an average of 9.13 kt per month, with the main NO_x-emitting sectors being power generation, transport and cement. Total emissions, as well as their share in the total NO_x budget, may have varied since then. This section compares our estimated emissions with local electricity generation and existing global inventories in order to provide a sectoral approach to NO_x emissions and their annual variability.

6.1 Comparison with electricity generation data

In Qatar, all electricity production comes from gas-fired power plants, with three plants located in the northeast (Ras Laffan area). Other gas power plants are located in the urban area of Doha and in the southeast of the country. Figure 11 shows the total electricity production and the share of the power plants in Ras Laffan between 2019 and 2021 as provided by Kahramaa. Data regarding the electricity generation by power plant in 2022 are not yet available. The electricity generation is 2 to 2.5 times higher during summer months than during winter months. This increased generation is mostly due to the use of air conditioning (Gastli et al., 2013), which is also captured in Fig. 9.

The inferred emissions have a behaviour that is similar to electricity generation, with higher emissions in the warmer months. The comparison of the time series of NO_x emissions and the electricity generation data for the 4-year period provides a correlation coefficient of $R^2 = 0.400$. This value is relatively low, but it should be noted that monthly emission maps can be very noisy due to averaging over too few days. For instance, in April 2019, the spatial distribution of emissions for this month shows non-negligible emissions in the central part of the country where no significant emitter is located. We can therefore consider it to be the case that the average is not calculated with enough data to limit noise effects. When we only keep in the analysis the mean

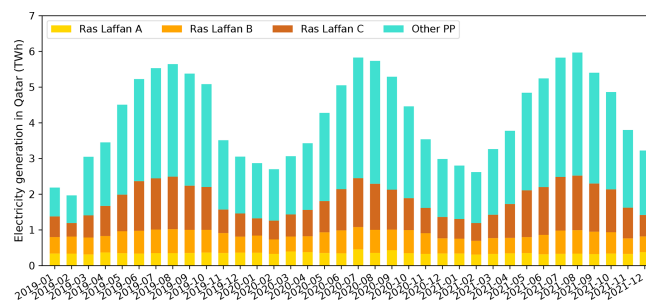


Figure 11. Electricity generation in Qatar from 2019 to 2021 according to the Planning and Statistics Authority reports. Generation from the three Ras Laffan power plants in the northeastern part of the country, is displayed in yellow, orange and brown, while generation from other power plants is displayed in light blue.

monthly emissions calculated on the basis of more than 18 d (the average over the 4-year period being 17.1), 19 points out of 48 are retained, and the correlation is improved, with a coefficient which then reaches $R^2 = 0.657$, with a slope of $1.773 \text{ t}_{\text{NO}_x} \text{ GWh}^{-1}$. This value would be equal to the emission factor of the power sector, provided that it was the only source of variable NO_x emissions during the months that are considered. This value must therefore be considered as an upper-limit estimate. Figure 12 shows the comparison between electricity generation and emissions in the two cases. The points that are retained in the second case mostly correspond to months with high emissions, notably in autumn. Among these 19 points, only 2 correspond to winter or spring months (December to May), whereas 7 correspond to summer months (June to August) and 10 to autumn months (September to November). The improved correlation must be interpreted with caution, but it might be possible that other NO_x-producing sectors have a seasonality which is the opposite to that of the power sector. If the transport sector has no particular seasonal cycle, it is possible that industry has a higher production during winter and spring months, leading to higher industrial NO_x emissions during this period. As

mentioned before, midday temperatures in summer are high in Qatar, preventing labour in outdoor activities, and this interpretation could be investigated. With the exception of the two cement plants in the west of the country, most of the industries are located in the urban area of Doha or Ras Laffan, where emissions from several sectors overlap over distances smaller than the resolution of TROPOMI.

The method can also be applied to a smaller area of the domain. The northeastern part of the country is interesting in this respect: it is very sparsely populated, and the human activity there is mainly associated with oil and gas activities and the production of electricity. In this region, three power plants (Ras Laffan A, B and C) have a total capacity of 3.35 GW and are responsible for about 45 % of the total electricity generation throughout the year, as shown in Fig. 11. These power plants are independent water and power plants (IWPPs), serving as both desalination plants and power plants. Other than these plants, the region also has gas liquefaction facilities as Qatar is a major producer of liquefied natural gas. Refineries are also present. In the life cycle of gas, only extraction and combustion are highly NO_x-emitting processes: emissions from midstream (liquefaction and transport) and downstream (refining) activities are 20 to 30 times lower per unit of fuel (Marais et al., 2022). As the oil and gas extraction processes are located outside this area (mostly offshore), it can be considered that the majority of the NO_x emitted in this region comes from the combustion of gas in the power plants. This is not the case for other power plants in the country, which are located in urban areas where emissions from different sectors overlap. We focus on this area and calculate the corresponding monthly emissions. The three power plants are located within the same pixel, and the difficulty for TROPOMI to visualize this region with good-quality measurements is less pronounced than for other regions identified in Sect. 5.3. Because Ras Laffan plants are not the only ones participating in the country's electricity generation, the use of load curves is no longer valid to infer total emissions in a given period, and only emissions at 13:30 can be considered. Assuming a correct calculation of emissions, the observed emissions display a Gaussian distribution around the power plants. Using a zonal cross-section of obtained emissions in a 28 km band centred around the mean latitude of the plants, we estimate the mean emissions by fitting a Gaussian curve $e_{\text{NO}_x}(\lambda) = B + \frac{E_0}{\sigma\sqrt{2\pi}} \exp\left(-\frac{(\lambda-\lambda_0)^2}{2\sigma^2}\right)$ to the profile, with B being the observed emissions above desert areas and seas, λ_0 being the mean longitude of the power plants, σ being the standard deviation (measured as an angle) and E_0 being the total emissions. λ is the zonal angle. The best approximation is displayed in Fig. 13.

Monthly profiles peak around the location of the power plants whose heights vary without displaying any particular seasonality. The fit of the averaged profile leads to a low positive background of 67.8 kg h⁻¹ per unit of band surface, i.e. about 0.390 mg m⁻² h⁻¹, and average emissions of 1.86 t h⁻¹

for the three power plants. This value is 1 order of magnitude similar than that of emissions for power plants in other regions estimated with the flux-divergence method (de Foy and Schauer, 2022; Sun, 2022). In particular, it corresponds approximately to the value reported by Beirle et al. (2023), which estimated an output of 1.81 t h⁻¹ despite various differences in the parameterization of the method.

Here, only a small part of the domain is considered, for which the power sector is by far the major contributor to NO_x emissions. It is therefore not necessary to consider the seasonality of the other sectors in the estimation of an emission factor, as was done earlier when the emissions of the whole domain were considered. However, as the scaling assumption can no longer be used, other assumptions must be made. One assumption would be that these plants serve as intermediate-load power plants: with 13:30 being a peak of consumption at any time of the year, the Ras Laffan plants would be running very close to their maximum capacity, and the annual variability of power generation by the three plants observed in Fig. 11 would be due to the decrease in power generation during low-demand hours. This would be consistent with the lack of seasonality detected in the monthly profiles in Fig. 13. In this case, comparing the emissions at 13:30 with the total capacity of the plants provides an emission factor of 0.557 t_{NO_x} GWh⁻¹. As the total capacity is used in the calculation, this value must be considered as a lower-limit estimate.

Another possible assumption is that the three plants are used as peak-load power plants: in this case, they would be used at 13:30 to respond to the daily peak. This use would increase with the height of the peak and therefore with the temperature. In this case, the annual variability of power generation by the three plants would be due to their variable use at 13:30. The absence of a clear annual variability in our TROPOMI-inferred emissions would be explained by the large uncertainties in the calculation of our emissions, which concern only six pixels of our domain. Here, the large share of the three power plants in the electricity production seems to rule out a peak-load functioning. However, it is also possible that some of the plants correspond to different functions within the national grid.

6.2 Comparison with emission inventories

We compare TROPOMI-derived NO_x emissions to the Emissions Database for Global Atmospheric Research (EDGARv6.1) for 2018 and the CAMS global anthropogenic emissions (CAMS-GLOB-ANT_v5.3) from 2019 to 2022. The two inventories provide 0.1° × 0.1° sectorial gridded emissions on a monthly basis. After aggregating the different sectors of activity, the CAMS-GLOB-ANT and EDGAR inventories directly provide the anthropogenic NO_x emissions over the same domain. Both inventories display NO_x emissions that are significantly higher than our estimates. According to CAMS-GLOB-ANT, the annual emissions for 2019,

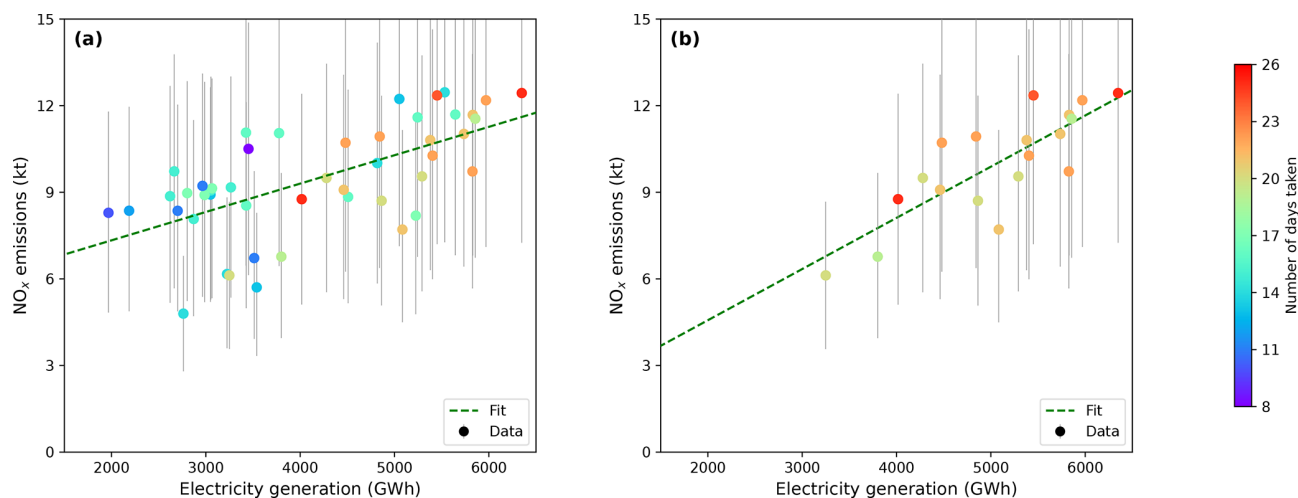


Figure 12. Comparison between monthly TROPOMI-derived NO_x emissions for the entire Qatar territory and corresponding electricity generation according to Planning and Statistics Authority reports. A linear regression between the two datasets is displayed with a dashed green line. **(a)** All months in the period 2019–2022 are included. **(b)** Months that are included are those for which inferred total emissions have been obtained with an averaging of 18 daily emissions or more. The colour scale represents the number of days involved in the calculation of points.

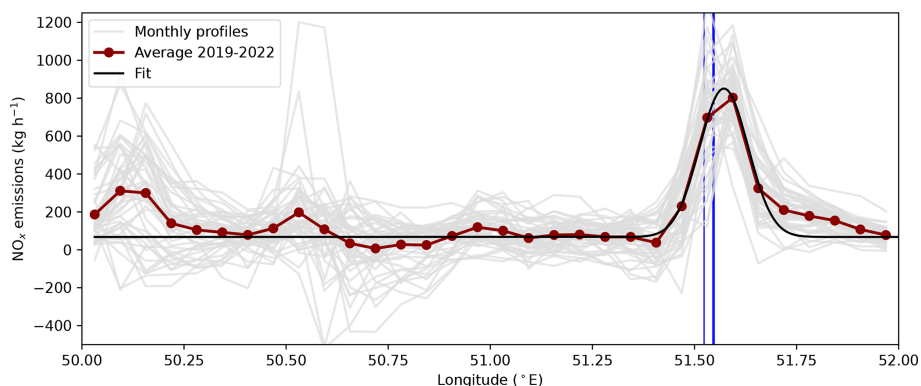


Figure 13. Zonal cross-sections of 13:30 NO_x emissions at the latitude of Ras Laffan power plants. The average profile for 2019–2022 is displayed in red, and the corresponding Gaussian fit is displayed in black. Individual monthly profiles are displayed in light grey. The positions of the three power plants are marked with vertical blue lines.

2020, 2021 and 2022 are 191.7, 191.8, 192.5 and 193.7 kt respectively, whereas we only estimate emissions of 111.5, 111.8, 114.4 and 121.0 kt for these same years. According to EDGAR, NO_x emissions are even higher, reaching 193.8 kt in 2018. It should be noted that the same version of EDGAR estimates emissions of 111.1 kt in 2007, which is similar to the reported terrestrial emissions for the same year, as well as our estimated emissions for 2019–2022.

The sectoral shares of emissions estimated by EDGAR and CAMS-GLOB-ANT differ. In EDGAR, the transport sector accounts for 42 % to 54 % of the emissions, whereas it has a nearly constant share of 50 % in CAMS-GLOB-ANT. In the remaining emissions, industry accounts for about 2.8 kt per month in both inventories. These emissions are slightly lower during summer, which can be interpreted as a lower

production due to a reduced outdoor activity at high temperatures. The corresponding share is more variable in EDGAR (between 13 % and 23 % of terrestrial emissions) than in CAMS-GLOB-ANT (about 17 % of terrestrial emissions). These values are lower than reported industrial shares for 2007, where the cement sector alone accounted for 23.4 % of total emissions. Finally, power sector emissions in both inventories account for a significant share of total emissions but with a higher value for EDGAR (35 % of the total budget for 2018) than for CAMS-GLOB-ANT (32 % of total emissions in 2019–2022). The two values are respectively higher and lower than the reported share for power emissions, which was estimated at 28.1 % for terrestrial emissions in 2007. Another major difference concerns the seasonal cycle of those power emissions. The two inventories do not

show any correlation with the corresponding electricity generation data. However, in 2018, EDGARv6.1 shows a pronounced variability, with extremes of 7.0 kt emitted in May and 3.5 kt in December (see the Supplement). The ratio between these two values remains lower than the ratio between the extremes of the monthly electricity generations, which has varied between 2.2 and 2.8 over the last 4 years, but it highlights a difference compared to the previous version of EDGAR (EDGARv5.0), which showed almost no seasonality in power emissions. This lack of seasonality is also found in the emissions of CAMS-GLOB-ANT_v5.3, which uses EDGARv5.0 as a basis. We also note that, while these seasonality differences between TROPOMI-inferred emissions and inventories were already highlighted for the previous versions of EDGAR and CAMS-GLOB-ANT in Egypt, the difference between mean annual NO_x emissions was much lower (Rey-Pommier et al., 2022).

6.3 Emission factor for the power sector

The report for emissions in 2007 indicates an emission factor for the power sector of 0.392 t_{NO_x} GWh⁻¹, and the corresponding power plants are still operating today. In the previous sections, we estimated an emission factor of 1.773 t_{NO_x} GWh⁻¹ using all monthly emissions in the internal mask and assuming the power sector was the only source of variable NO_x emissions. We also estimated a value of 0.557 t_{NO_x} GWh⁻¹ for Ras Laffan power plants using mean emissions at 13:30 under the hypothesis of an intermediate-load power plant functioning. To infer emission factors from inventory estimates, power emissions in EDGAR and CAMS-GLOB-ANT and total electricity generation provided by the Planning and Statistics Authority (PSA) between 2018 and 2022 can also be used to infer emission factors of 1.406 and 1.219 t_{NO_x} GWh⁻¹ respectively. Table 1 summarizes all the different emission factors that have been calculated. Even though EDGAR's emission factor is particularly high compared to other estimates, the five listed values are plausible, as the majority of gas-fired power plants have a NO_x emission factor value between 0.1 and 10 t_{NO_x} GWh⁻¹ (Miller, 2004).

The comparison between these different emission factors should be made with caution. The factor reported by the report for 2007 emissions takes into account all of the power plants in the country, the oldest having been built in 1980. Moreover, some units of one of the Ras Laffan plants were built between 2010 and 2011, i.e. after the publication of the report. It is also possible that other power plants have been upgraded in the last years. Finally, the reported emission factor for 2007 accounts for the public electricity production and the water production, but the monthly reports from Kahramaa do not specify whether the electricity generation from the Ras Laffan power plants accounts for the large amount of electricity that is used in desalination processes (Kahramaa, 2023). Monthly reports show that the water production from

the IWPPs in the country does not have a clear annual cycle, with the production generally ranging between 50 × 10⁶ and 60 × 10⁶ m³ per month in the entire country. The amount of electricity needed for this water production varies with the technologies used in the IWPPs and accounts for about 20 % of the consumption in total electricity (Okonkwo et al., 2021). Consequently, if the electricity used for water production is not accounted for in the electricity generation for monthly reports, then all inferred emission factors are overestimated.

7 Uncertainties and assessment of results

The long time series of average NO₂ concentrations in cities in several countries with similar economic and industrial developments (Dubai, Manama, Kuwait City) show a stagnation of NO_x levels over the period 2005–2014 (Lelieveld et al., 2015). It is therefore not clear whether the NO_x emissions of the country in 2019–2022 increased from their value in 2007, as suggested by CAMS and EDGAR, or decreased, as our TROPOMI-based estimates seem to suggest. We do not know exactly how parameters in EDGARv6.1 and CAMS-GLOB-ANT_v5.3 are estimated in order to calculate NO_x emissions, which means we cannot conduct a discussion on such bottom-up estimates accordingly. However, we can identify several factors that could influence our top-down NO_x emissions. The following aspects can be considered:

- As discussed in Sect. 5.3, a large portion of the territory, which includes some of the most emissive facilities in the country, is not visible to TROPOMI with high-quality data, and emissions from very emissive pixels might be underestimated. As this situation only occurs from 2019 to 2021, the magnitude of the induced underestimation is the difference between inferred emissions in 2022 and inferred emissions in 2019–2021, i.e. about 6 %.
- TROPOMI retrievals are sometimes biased due to poor estimation of the air mass factor or local effects under particular vertical distribution conditions (Griffin et al., 2019; Lorente et al., 2019; Judd et al., 2020; Wang et al., 2021). It should be noted that the latest versions of TROPOMI (v2.x) have tropospheric VCDs that are between 10 % and 40 % larger than the first versions (v1.x), depending on the level of pollution and the season (van Geffen et al., 2022). The chemical transport model TM5, which is used in the retrieval of the operational TROPOMI data, has been shown to underestimate surface level pollution while overestimating NO₂ at higher levels above the sea (Latsch et al., 2023; Rieß et al., 2023). Such a bias is probably not negligible and probably accounts for a significant part of the difference between our estimates and inventories but is also within our estimates as surface albedo values differ between desert areas and urban zones.

Table 1. NO_x emission factors for electricity production inferred from different sources and methods. The value is calculated from monthly emissions and electricity generation, fluxes at 13:30, and capacities, or it is directly reported by Qatar authorities.

Year(s)	Source	Data for NO _x emissions	Data for power	Method	Emission factor (tNO _x GWh ⁻¹)
2007	All PPs	Reported emission factor (Initial National Communication to the UNFCCC)			0.392
2018	All PPs	EDGARv6.1 inventory NO _x emissions	Annual power generation (PSA)	Ratio between total power emissions and electricity generation	1.406
2019 to 2022	All PPs	CAMS-GLOB-ANT_v5.3 inventory NO _x emissions	Monthly power generation (PSA)	Ratio between total power emissions and electricity generation	1.219
2019 to 2022	Internal mask	Monthly TROPOMI-inferred NO _x emissions	Monthly power generation (PSA)	Linear fit between monthly power emissions and electricity generation	1.773
2019 to 2022	Ras Laffan power plants	13:30 TROPOMI-inferred NO _x emissions	Power plant capacities (PSA)	Gaussian fit of zonal cross-section for Ras Laffan power plants	0.557

- The vertical levels on which parameters in Eq. (1) are estimated might be incorrect. Most studies use values averaged within the PBL, which is higher in summer (Lorente et al., 2019; Lama et al., 2020), or averaged within a fixed vertical layer (Beirle et al., 2019). Here, we interpolated the fields of w , T and [OH] using the first pressure levels in ERA5 and CAMS at a mean pressure of 987.5 hPa. As Qatar is a flat country, this level corresponds to an altitude between 220 and 250 m. Because vertical transport of NO_x, which is emitted mainly from combustion engines and industrial stacks, is generally minor compared to horizontal transport (Sun, 2022), NO_x is confined to these first 100 m above ground level. In Egypt, Rey-Pommier et al. (2022) have shown that the consideration of higher levels decreases the mean temperature, which tends to increase emissions, balanced by the decrease of mean OH concentrations with altitude, which tends to decrease the sink. The net effect would be a decrease of emissions by a few percents during most of the year.
 - The NO_x-to-NO₂ ratio might be locally underestimated. The conversion of NO to NO₂ by the reaction with O₃ is balanced by the photolysis of NO₂, which reforms NO, leading to a stabilization of the ratio a few kilometres downwind of the source. The stationary regime can also be displaced by the presence of volatile organic compounds. Near important sources of emissions, which mainly produce NO, a high NO_x-to-NO₂ ratio should be expected. We can therefore consider that, for pixels containing hotspots close to their boundaries, such as power plants, it should be much higher than the chosen value of 1.32 (Hanrahan, 1999; Goldberg et al., 2022), leading to an underestimation of our emissions locally. With power plants concentrating a large share of the NO_x emissions in our study, this effect is probably not negligible and probably accounts for a large part of the difference between our estimates and inventories.
 - The sink term might be underestimated or overestimated. If the transport term is assumed to be estimated correctly, an underestimation of the sink term would lead to significant negative emissions in many parts of the domain, while an overestimation would lead to non-emitting areas with NO_x emissions that are higher than noise. None of these effects seem to appear for averaged emissions for the 2019–2022 period, but monthly maps show significant portions of the territory with negative emissions in winter and spring months, while summer months display abnormally high emissions over deserts and seas. Those effects are not visible for most of the autumn months. We can therefore assume that the sink term is slightly underestimated in winter and spring months and overestimated in summer months due to errors in the estimation of OH in CAMS and/or the presence of additional sinks in summer. Accounting for this effect would not change the averaged emissions for the period 2019–2022 but would reduce the seasonality observed in Fig. 6. The emission factor calculated from emissions in the internal mask would also be reduced.
- These effects must be taken into account to understand the differences between our model, reported emissions and inventory emissions. The uncertainties used here must also be considered. NO_x emissions, as estimated with the flux-divergence method, are calculated with the use of several quantities. The uncertainty ranges shown in Figs. 10 and 12 are calculated from uncertainty statistics whose references are presented in this section, assuming that they correspond to standard deviations. The uncertainty of tropospheric NO₂ columns under polluted conditions is dominated by the sensitivity of satellite observations to air masses in the lower troposphere, expressed by the AMF, and the corresponding relative uncertainty is of the order of 30 % (Boersma et al., 2004) and is likely related to the a priori profiles used within the operational retrieval that do not reflect well the concentration peak of NO₂ near the ground. For the Middle-Eastern region,

the impact of the a priori profile is less critical as surface albedo is generally high and cloud fractions are generally low. Thus, we do not expect a bias of this importance, and we consider a relative uncertainty of 30 % for the tropospheric column to be reasonable. For the wind module, we assume an uncertainty of 3 m s⁻¹ for both the zonal and meridional wind components. For OH concentrations, the analysis of different methods conducted by Huijnen et al. (2019) showed smaller differences for low latitudes than for extratropics, but these were still significant. We thus take a relative uncertainty of 30 % for OH concentration. For the reaction rate k_{mean} , we use the value of the corresponding relative uncertainty, as estimated by Burkholder et al. (2020).

8 Conclusion

In this study, we investigated the potential of a top-down model of NO_x emissions based on TROPOMI retrievals and a flux-divergence scheme applied at high resolution over Qatar for the last 4 years (2019–2022). This scheme requires different parameters to be calculated and consists of the calculation of a transport term that uses horizontal wind and the calculation of a sink term that requires temperature data and OH concentration to illustrate the chemical loss of NO_x. Results illustrate the difference between localized and diffuse sources of NO_x. For diffuse sources such as the Doha urban area, the transport term and the sink term similarly contribute to the total NO_x budget, whereas the transport term is higher than the sink term for localized sources such as the gas power plants located in the northeast of the country. The emissions from other hotspots, such as cement plants in the western part of the country, could not be correctly estimated from 2019 to 2021 due to unavailability of high-quality TROPOMI retrievals. Our estimated NO_x emissions show a weekly variability which is consistent with the social norms of the country and an annual variability which is consistent with its electricity generation. In this study, estimated emissions are similar to reported emissions in 2007, but they are 1.67 times lower than emissions in the CAMS-GLOB-ANT_v5.3 inventory for 2019–2022 and 1.68 times lower than emissions in EDGARv6.1 for 2018. They have an annual cycle whose relative amplitude is higher than those two inventories. These notable differences may be subject to further discussion regarding sectoral activity data and emission factors used in global inventories. Finally, this study is also an attempt to retrieve the NO_x emission factor of the power sector. This top-down estimation is made possible by the desert features of Qatar, which allow us to consider only one chemical sink, and also by the low diversity of its economy in which the power sector is the major source of variable NO_x. An emission factor is also estimated for a group of isolated gas power plants. The emission factors are 1.42 and 4.52 times higher than the value reported for 2007. Moreover, the emission factor of the entire power sector is higher than

that of the three isolated gas power plants, indicating higher emission factors for other power plants in Doha. Although several limitations exist in the estimation of these results, we believe that such a calculation can be reproduced in other countries and for power plants that share similar characteristics. Overall, this study highlights the potential of TROPOMI to compensate for non-existent, inaccurate or outdated inventories by providing low-latency emission estimates. The development of similar applications is likely to provide a better monitoring of global anthropogenic emissions, therefore helping countries to report their emissions of air pollutants and greenhouse gases as part of their strategies and obligations to tackle air pollution issues and climate change.

Code availability. Code will be made available on request.

Data availability. The TROPOMI Sentinel 5P Product Algorithm Laboratory (S5P-PAL) reprocessed data (processor version 2.3.1) from January 2019 to October 2020 have been used. The OFFL stream was used afterwards using processor versions 2.3.1 and 2.4.0 from November 2022. The TROPOMI NO₂ product is publicly available on the TROPOMI open hub (<http://www.tropomi.eu/data-products/data-access>, TROPOMI Data Hub, 2023) while the S5P-PAL reprocessed data can be found on the S5P-PAL data portal (<https://data-portal.s5p-pal.com>, ESA: , 2023). CAMS data can be downloaded from the Copernicus Climate Data Store (<https://ads.atmosphere.copernicus.eu/cdsapp#!/dataset/cams-global-atmospheric-composition-forecasts>,). The European Centre for Medium-Range Weather Forecasts (ECMWF) ERA5 reanalysis can be downloaded from the Copernicus Climate Data Store (<https://cds.climate.copernicus.eu/cdsapp#!/dataset/reanalysis-era5-pressure-levels-monthly-means>,). CAMS-GLOB-ANT_v5.3 data are available at <https://eccad.sedoo.fr/#/metadata/479> (ECCAD-AERIS, 2023). EDGARv6.1 Global Air Pollutant Emissions are provided by https://edgar.jrc.ec.europa.eu/dataset_ap61 (European Commission, 2023).

Supplement. The supplement related to this article is available online at: <https://doi.org/10.5194/acp-23-13565-2023-supplement>.

Author contributions. AR analysed the data, prepared the main software code and wrote the paper. FC provided the TROPOMI NO₂ data product and corresponding gridded maps. ISB provided time series of electricity consumption. PC, TC, JK and JS contributed to the improvement of the method and the interpretation of the results. All the authors read and agreed on the published version of the paper.

Competing interests. The contact author has declared that none of the authors has any competing interests.

Disclaimer. Publisher's note: Copernicus Publications remains neutral with regard to jurisdictional claims made in the text, published maps, institutional affiliations, or any other geographical representation in this paper. While Copernicus Publications makes every effort to include appropriate place names, the final responsibility lies with the authors.

Financial support. This study has been funded by the European Union's Horizon 2020 research and innovation programme under grant agreement no. 856612 (EMME-CARE) and partially under grant agreement no. 958927 (Prototype System for a Copernicus CO₂ Service (CoCO₂)).

Review statement. This paper was edited by Bryan N. Duncan and reviewed by two anonymous referees.

References

- Al-Attiyah Foundation: Gear change: Vehicle fuel efficiency in the GCC, <https://www.abhafoundation.org/media-uploads/rpapers/Research%20series-17-Date-01-2018-Fuel%20Efficiency%20GCC.pdf> (last access: 25 October 2023), 2018.
- Bayram, I. S., Saffouri, F., and Koc, M.: Generation, analysis, and applications of high resolution electricity load profiles in Qatar, *J. Clean. Prod.*, 183, 527–543, 2018.
- Beirle, S., Borger, C., Dörner, S., Li, A., Hu, Z., Liu, F., Wang, Y., and Wagner, T.: Pinpointing nitrogen oxide emissions from space, *Sci. Adv.*, 5, eaax9800, <https://doi.org/10.1126/sciadv.aax9800>, 2019.
- Beirle, S., Borger, C., Jost, A., and Wagner, T.: Improved catalog of NO_x point source emissions (version 2), *Earth Syst. Sci. Data*, 15, 3051–3073, <https://doi.org/10.5194/essd-15-3051-2023>, 2023.
- Boersma, K., Eskes, H., and Brinksma, E.: Error analysis for tropospheric NO₂ retrieval from space, *J. Geophys. Res.-Atmos.*, 109, D04311, <https://doi.org/10.1029/2003JD003962>, 2004.
- Bovensmann, H., Burrows, J., Buchwitz, M., Frerick, J., Noel, S., Rozanov, V., Chance, K., and Goede, A.: SCIAMACHY: Mission objectives and measurement modes, *J. Atmos. Sci.*, 56, 127–150, 1999.
- Burkholder, J., Sander, S., Abbatt, J., Barker, J., Cappa, C., Crouse, J., Dibble, T., Huie, R., Kolb, C., Kurylo, M., Orkin, V. L., Percival, C. J., Wilmouth, D. M., and Wine, P. H.: Chemical kinetics and photochemical data for use in atmospheric studies, Evaluation Number 19, JPL Publication 19-5, Jet Propulsion Laboratory, Pasadena, NASA, CA, <http://jpldataeval.jpl.nasa.gov> (last access: 23 August 2022), 2020.
- Burnett, R. T., Stieb, D., Brook, J. R., Cakmak, S., Dales, R., Raizenne, M., Vincent, R., and Dann, T.: Associations between short-term changes in nitrogen dioxide and mortality in Canadian cities, *Arch. Environ. Health*, 59, 228–236, 2004.
- Butenhoff, C. L., Khalil, M. A. K., Porter, W. C., Al-Sahafi, M. S., Almazroui, M., and Al-Khalaf, A.: Evaluation of ozone, nitrogen dioxide, and carbon monoxide at nine sites in Saudi Arabia during 2007, *J. Air Waste Manage.*, 65, 871–886, 2015.
- Celarié, E., Brinksma, E., Gleason, J., Veeffkind, J., Cede, A., Herman, J., Ionov, D., Goutail, F., Pommereau, J.-P., Lambert, J.-C., van Roozendaal, M., Pinardi, G., Wittrock, F., Schönhardt, A., Richter, A., Ibrahim, O. W., Wagner, T., Bojkov, B., Mount, G., Spinei, E., Chen, C. M., Pongetti, T. J., Sander, S. P., Bucseles, E. J., Wenig, M. O., Swart, D. P. J., Volten, H., Kroon, M., and Levelt, P. F.: Validation of Ozone Monitoring Instrument nitrogen dioxide columns, *J. Geophys. Res.-Atmos.*, 113, D15S15, <https://doi.org/10.1029/2007JD008908>, 2008.
- de Foy, B. and Schauer, J. J.: An improved understanding of NO_x emissions in South Asian megacities using TROPOMI NO₂ retrievals, *Environ. Res. Lett.*, 17, 024006, <https://doi.org/10.1088/1748-9326/ac48b4>, 2022.
- Demetillo, M. A. G., Navarro, A., Knowles, K. K., Fields, K. P., Geddes, J. A., Nowlan, C. R., Janz, S. J., Judd, L. M., Al-Saadi, J., Sun, K., McDonald, B. C., Diskin, G. S., and Pusede, S. E.: Observing nitrogen dioxide air pollution inequality using high-spatial-resolution remote sensing measurements in Houston, Texas, *Environ. Sci. Technol.*, 54, 9882–9895, 2020.
- ECCAD-AERIS: CAMS-GLOB-ANT_v5.3 data [data set], <https://eccad.sedoo.fr/#/metadata/479>, last access: 5 October 2023.
- ECMWF: CAMS data, Copernicus Climate Data Store [data set], <https://ads.atmosphere.copernicus.eu/cdsapp#!/dataset/cams-global-atmospheric-composition-forecasts>, last access: 5 October 2023a.
- ECMWF: ERA5 reanalysis, Copernicus Climate Data Store [data set], <https://cds.climate.copernicus.eu/cdsapp#!/dataset/reanalysis-era5-pressure-levels-monthly-means>, last access: 5 October 2023.
- Ehnhalt, D. H., Rohrer, F., and Wahner, A.: Sources and distribution of NO_x in the upper troposphere at northern mid-latitudes, *J. Geophys. Res.-Atmos.*, 97, 3725–3738, 1992.
- EIA: Natural gas, <https://www.eia.gov/international/data/world/natural-gas/dry-natural-gas-reserves> (last access: 25 October 2023), 2021.
- EIA: Analysis - Energy Sector Highlights, <https://www.eia.gov/international/data/country/QAT> (last access: 25 October 2023), 2022.
- Eskes, H., van Geffen, J., Boersma, F., Eichmann, K., Apituley, A., Pedernana, M., Sneep, M., Veeffkind, J., and Loyola, D.: Sentinel-5 precursor/TROPOMI Level 2 Product User Manual Nitrogen dioxide, Royal Netherlands Meteorological Institute, <https://sentinel.esa.int/documents/247904/2474726/Sentinel-5P-Level-2-Product-User-Manual-Nitrogen-Dioxide.pdf> (last access: 25 October 2023), 2022.
- European Commission: EDGAR v6.1 Global Air Pollutant Emissions [data set], https://edgar.jrc.ec.europa.eu/dataset_ap61, last access: 25 October 2023.
- Gastli, A., Charabi, Y., Alammari, R. A., and Al-Ali, A. M.: Correlation between climate data and maximum electricity demand in Qatar, in: 2013 7th IEEE GCC Conference and Exhibition (GCC), Doha, Qatar, 17–20 November 2013, IEEE, 565–570, <https://doi.org/10.1109/IEEEGCC.2013.6705841>, 2013.
- Goldberg, D. L., Harkey, M., de Foy, B., Judd, L., Johnson, J., Yarwood, G., and Holloway, T.: Evaluating NO_x emissions and their effect on O₃ production in Texas using TROPOMI NO₂ and HCHO, *Atmos. Chem. Phys.*, 22, 10875–10900, <https://doi.org/10.5194/acp-22-10875-2022>, 2022.

- Graedel, T., Farrow, L., and Weber, T.: Kinetic studies of the photochemistry of the urban troposphere, *Atmos. Environ.*, 10, 1095–1116, 1976.
- Granier, C., Darras, S., Denier van der Gon, H., Doubalova, J., Elguindi, N., Galle, B., Gauss, M., Guevara, M., Jalkanen, J.-P., Kuenen, J., Liousse, C., Quack, B., Simpson, D., and Sindelarova, K.: The Copernicus Atmosphere Monitoring Service global and regional emissions (April 2019 version), Copernicus Atmosphere Monitoring Service (CAMS) report, 2019, <https://doi.org/10.24380/d0bn-kx16>, 2019.
- Griffin, D., Zhao, X., McLinden, C. A., Boersma, F., Bourassa, A., Dammers, E., Degenstein, D., Eskes, H., Fehr, L., Fioletov, V., Hayden, K., Kharol, S. K., Li, S.-M., Makar, P., Martin, R. V., Mihele, C., Mittermeier, R. L., Krotkov, N., Sneep, M., Lamsal, L. N., ter Linden, M., van Geffen, J., Veeffkind, P., and Wolde, M.: High-resolution mapping of nitrogen dioxide with TROPOMI: First results and validation over the Canadian oil sands, *Geophys. Res. Lett.*, 46, 1049–1060, 2019.
- Hale, T., Angrist, N., Goldszmidt, R., Kira, B., Petherick, A., Phillips, T., Webster, S., Cameron-Blake, E., Hallas, L., Majumdar, S., and Tatlow, H.: A global panel database of pandemic policies (Oxford COVID-19 Government Response Tracker), *Nature Human Behaviour*, 5, 529–538, 2021.
- Hanrahan, P. L.: The plume volume molar ratio method for determining NO₂/NO_x ratios in modeling—Part II: Evaluation studies, *J. Air Waste Manage.*, 49, 1332–1338, 1999.
- He, M. Z., Kinney, P. L., Li, T., Chen, C., Sun, Q., Ban, J., Wang, J., Liu, S., Goldsmith, J., and Kioumourtoglou, M.-A.: Short-and intermediate-term exposure to NO₂ and mortality: a multi-county analysis in China, *Environ. Pollut.*, 261, 114165, <https://doi.org/10.1016/j.envpol.2020.114165>, 2020.
- Hersbach, H., Bell, B., Berrisford, P., et al.: The ERA5 global reanalysis, *Q. J. Roy. Meteor. Soc.*, 146, 1999–2049, 2020.
- Hoelzemann, J. J., Schultz, M. G., Brasseur, G. P., Granier, C., and Simon, M.: Global Wildland Fire Emission Model (GWEM): Evaluating the use of global area burnt satellite data, *J. Geophys. Res.-Atmos.*, 109, D14S04, <https://doi.org/10.1029/2003JD003666>, 2004.
- Hoesly, R. M., Smith, S. J., Feng, L., Klimont, Z., Janssens-Maenhout, G., Pitkanen, T., Seibert, J. J., Vu, L., Andres, R. J., Bolt, R. M., Bond, T. C., Dawidowski, L., Kholod, N., Kurokawa, J.-I., Li, M., Liu, L., Lu, Z., Moura, M. C. P., O'Rourke, P. R., and Zhang, Q.: Historical (1750–2014) anthropogenic emissions of reactive gases and aerosols from the Community Emissions Data System (CEDS), *Geosci. Model Dev.*, 11, 369–408, <https://doi.org/10.5194/gmd-11-369-2018>, 2018.
- Huijnen, V., Pozzer, A., Arteta, J., Brasseur, G., Bouarar, I., Chabrilat, S., Christophe, Y., Doumbia, T., Flemming, J., Guth, J., Josse, B., Karydis, V. A., Marécal, V., and Pelletier, S.: Quantifying uncertainties due to chemistry modelling – evaluation of tropospheric composition simulations in the CAMS model (cycle 43R1), *Geosci. Model Dev.*, 12, 1725–1752, <https://doi.org/10.5194/gmd-12-1725-2019>, 2019.
- Jaeglé, L., Steinberger, L., Martin, R. V., and Chance, K.: Global partitioning of NO_x sources using satellite observations: Relative roles of fossil fuel combustion, biomass burning and soil emissions, *Faraday Discuss.*, 130, 407–423, 2005.
- Janssens-Maenhout, G., Crippa, M., Guizzardi, D., Muntean, M., Schaaf, E., Dentener, F., Bergamaschi, P., Pagliari, V., Olivier, J. G. J., Peters, J. A. H. W., van Aardenne, J. A., Monni, S., Doering, U., Petrescu, A. M. R., Solazzo, E., and Oreggioni, G. D.: EDGAR v4.3.2 Global Atlas of the three major greenhouse gas emissions for the period 1970–2012, *Earth Syst. Sci. Data*, 11, 959–1002, <https://doi.org/10.5194/essd-11-959-2019>, 2019.
- Judd, L. M., Al-Saadi, J. A., Szykman, J. J., Valin, L. C., Janz, S. J., Kowalewski, M. G., Eskes, H. J., Veeffkind, J. P., Cede, A., Mueller, M., Gebetsberger, M., Swap, R., Pierce, R. B., Nowlan, C. R., Abad, G. G., Nehrir, A., and Williams, D.: Evaluating Sentinel-5P TROPOMI tropospheric NO₂ column densities with airborne and Pandora spectrometers near New York City and Long Island Sound, *Atmos. Meas. Tech.*, 13, 6113–6140, <https://doi.org/10.5194/amt-13-6113-2020>, 2020.
- Kahramaa: Qatar General Electricity and Water Corporation, <https://www.km.qa/MediaCenter/Pages/Publications.aspx> (last access: 25 October 2023), 2023.
- Lama, S., Houweling, S., Boersma, K. F., Eskes, H., Aben, I., Denier van der Gon, H. A. C., Krol, M. C., Dolman, H., Borsdorff, T., and Lorente, A.: Quantifying burning efficiency in megacities using the NO₂/CO ratio from the Tropospheric Monitoring Instrument (TROPOMI), *Atmos. Chem. Phys.*, 20, 10295–10310, <https://doi.org/10.5194/acp-20-10295-2020>, 2020.
- Latsch, M., Richter, A., and Burrows, J. P.: Improving the detection of global NO_x emissions from shipping in S5P/TROPOMI data, EGU General Assembly, Vienna, Austria, Online, 23–28 April 2023, EGU23-5353, <https://doi.org/10.5194/egusphere-egu23-5353>, 2023.
- Lelieveld, J., Beirle, S., Hörmann, C., Stenchikov, G., and Wagner, T.: Abrupt recent trend changes in atmospheric nitrogen dioxide over the Middle East, *Science Advances*, 1, e1500498, <https://doi.org/10.1126/sciadv.1500498>, 2015.
- Lelieveld, J., Gromov, S., Pozzer, A., and Taraborrelli, D.: Global tropospheric hydroxyl distribution, budget and reactivity, *Atmos. Chem. Phys.*, 16, 12477–12493, <https://doi.org/10.5194/acp-16-12477-2016>, 2016.
- Levy, H.: Normal atmosphere: Large radical and formaldehyde concentrations predicted, *Science*, 173, 141–143, 1971.
- Li, M., Karu, E., Brenninkmeijer, C., Fischer, H., Lelieveld, J., and Williams, J.: Tropospheric OH and stratospheric OH and Cl concentrations determined from CH₄, CH₃Cl, and SF₆ measurements, *npj Climate and Atmospheric Science*, 1, 1–7, 2018.
- Lin, J.-T.: Satellite constraint for emissions of nitrogen oxides from anthropogenic, lightning and soil sources over East China on a high-resolution grid, *Atmos. Chem. Phys.*, 12, 2881–2898, <https://doi.org/10.5194/acp-12-2881-2012>, 2012.
- Lorente, A., Boersma, K., Eskes, H., Veeffkind, J., Van Geffen, J., De Zeeuw, M., Denier Van Der Gon, H., Beirle, S., and Krol, M.: Quantification of nitrogen oxides emissions from build-up of pollution over Paris with TROPOMI, *Sci. Rep.-UK*, 9, 1–10, 2019.
- Mansouri Daneshvar, M. R. and Hussein Abadi, N.: Spatial and temporal variation of nitrogen dioxide measurement in the Middle East within 2005–2014, *Modeling Earth Systems and Environment*, 3, 1–9, 2017.
- Marais, E. A., Akker, O., and Wiedinmyer, C.: Greenhouse gas and air pollutant emissions from power barges (powerships), *Environmental Science: Advances*, 1, 164–169, 2022.

- Miller, P. J.: North American power plant air emissions, Commission for Environmental Cooperation of North America, ISBN 978-2-89700-008-0, 2004.
- Müller, J.-F. and Stavrou, T.: Inversion of CO and NO_x emissions using the adjoint of the IMAGES model, *Atmos. Chem. Phys.*, 5, 1157–1186, <https://doi.org/10.5194/acp-5-1157-2005>, 2005.
- Okonkwo, E. C., Abdullatif, Y. M., and Tareq, A.-A.: A nano-material integrated technology approach to enhance the energy-water-food nexus, *Renew. Sust. Energ. Rev.*, 145, 111118, <https://doi.org/10.1016/j.rser.2021.111118>, 2021.
- OPEC: OPEC Annual Statistical Bulletin 2019, ISSN 0475-0608, https://www.opec.org/opec_web/static_files_project/media/downloads/publications/ASB_2019.pdf (last access: 25 October 2023), 2020.
- Osipov, S., Chowdhury, S., Crowley, J. N., Tadic, I., Drewnick, F., Borrmann, S., Eger, P., Fachinger, F., Fischer, H., Predybaylo, E., Fnais, M., Harder, H., Pikridas, M., Vouterakos, P., Pozzer, A., Sciare, J., Ukhov, A., Stenchikov, G. L., Williams, J., and Lelieveld, J.: Severe atmospheric pollution in the Middle East is attributable to anthropogenic sources, *Communications Earth & Environment*, 3, 1–10, 2022.
- PSA: Planning and Statistics Authority, Qatar Monthly Statistics, <https://www.psa.gov.qa/en/statistics1/Pages/default.aspx> (last access: 25 October 2023), 2023.
- Rey-Pommier, A., Chevallier, F., Ciais, P., Broquet, G., Christoudias, T., Kushta, J., Hauglustaine, D., and Sciare, J.: Quantifying NO_x emissions in Egypt using TROPOMI observations, *Atmos. Chem. Phys.*, 22, 11505–11527, <https://doi.org/10.5194/acp-22-11505-2022>, 2022.
- Richter, A. and Burrows, J.: Tropospheric NO₂ from GOME measurements, *Adv. Space Res.*, 29, 1673–1683, 2002.
- Rieß, T. C. V. W., van Vliet, J., Van Roy, W., de Laat, J., Dammers, E., and Boersma, F.: Aircraft validation reveals a 20% low bias in TROPOMI NO₂ over sea caused by TM5 a priori profiles, EGU General Assembly, Vienna, Austria, Online, 23–28 April 2023, EGU23-13654, <https://doi.org/10.5194/egusphere-egu23-13654>, 2023.
- Rohrer, F. and Berresheim, H.: Strong correlation between levels of tropospheric hydroxyl radicals and solar ultraviolet radiation, *Nature*, 442, 184–187, 2006.
- ESA: S5P-PAL Data Portal, NO₂ product, S5P-PAL Data Portal [data set], <https://data-portal.s5p-pal.com/>, last access: 5 October 2023.
- Saw, G. K., Dey, S., Kaushal, H., and Lal, K.: Tracking NO₂ emission from thermal power plants in North India using TROPOMI data, *Atmos. Environ.*, 259, 118514, <https://doi.org/10.1016/j.atmosenv.2021.118514>, 2021.
- Seinfeld, J. H.: Urban air pollution: state of the science, *Science*, 243, 745–752, 1989.
- Seinfeld, J. H. and Pandis, S. N.: Atmospheric chemistry and physics from air pollution to climate change, 2nd Edn., John Wiley & Sons, New York, ISBN-13 978-0-471-72017-1, 2006.
- Shikwambana, L., Mhangara, P., and Mbatha, N.: Trend analysis and first time observations of sulphur dioxide and nitrogen dioxide in South Africa using TROPOMI/Sentinel-5P data, *Int. J. Appl. Earth Obs.*, 91, 102130, <https://doi.org/10.1016/j.jag.2020.102130>, 2020.
- Stavrou, T., Müller, J.-F., Bauwens, M., Boersma, K., and van Geffen, J.: Satellite evidence for changes in the NO₂ weekly cycle over large cities, *Sci. Rep.-UK*, 10, 1–9, 2020.
- Sun, K.: Derivation of Emissions From Satellite-Observed Column Amounts and Its Application to TROPOMI NO₂ and CO Observations, *Geophys. Res. Lett.*, 49, e2022GL101102, <https://doi.org/10.1029/2022GL101102>, 2022.
- Tomtom: TomTom, Doha traffic, Qatar, https://www.tomtom.com/en_gb/traffic-index/doha-traffic/ (last access: 28 September 2022), 2023.
- TROPOMI Data Hub: TROPOMI NO₂ product, TROPOMI Open hub [data set], <https://www.tropomi.eu/data-products/nitrogen-dioxide>, last access: 5 October 2023.
- Ministry of Environment, Qatar: First National Communication of Qatar to the United Nations Framework Convention on Climate Change, <https://unfccc.int/resource/docs/natc/qatnc1.pdf> (last access: 25 October 2023), 2011.
- U.S. EPA: Integrated science assessment for oxides of nitrogen – Health Criteria (Final Report, Jan 2016), US Environmental Protection Agency, Washington, DC, EPA/600/R-15/068, 2016.
- Valin, L. C., Russell, A. R., Hudman, R. C., and Cohen, R. C.: Effects of model resolution on the interpretation of satellite NO₂ observations, *Atmos. Chem. Phys.*, 11, 11647–11655, <https://doi.org/10.5194/acp-11-11647-2011>, 2011.
- van Geffen, J., Eskes, H., Compennolle, S., Pinardi, G., Verhoelst, T., Lambert, J.-C., Sneep, M., ter Linden, M., Ludewig, A., Boersma, K. F., and Veefkind, J. P.: Sentinel-5P TROPOMI NO₂ retrieval: impact of version v2.2 improvements and comparisons with OMI and ground-based data, *Atmos. Meas. Tech.*, 15, 2037–2060, <https://doi.org/10.5194/amt-15-2037-2022>, 2022.
- Vandaele, A. C., Hermans, C., Simon, P. C., Carleer, M., Colin, R., Fally, S., Merienne, M.-F., Jenouvrier, A., and Coquart, B.: Measurements of the NO₂ absorption cross-section from 42 000 cm⁻¹ to 10 000 cm⁻¹ (238–1000 nm) at 220 K and 294 K, *J. Quant. Spectrosc. Ra.*, 59, 171–184, 1998.
- van Vuuren, D. P., Bouwman, L. F., Smith, S. J., and Dentener, F.: Global Projections for Anthropogenic Reactive Nitrogen Emissions to the Atmosphere: An Assessment of Scenarios in the Scientific Literature, *Curr. Opin. Env. Sust.*, 3, 359–369, 2011.
- Wang, Y., Yuan, Q., Li, T., Zhu, L., and Zhang, L.: Estimating daily full-coverage near surface O₃, CO, and NO₂ concentrations at a high spatial resolution over China based on S5P-TROPOMI and GEOS-FP, *ISPRS J. Photogramm.*, 175, 311–325, 2021.
- Wolfe, G. M., Nicely, J. M., St. Clair, J. M., Hanisco, T. F., Liao, J., Oman, L. D., Brune, W. B., Miller, D., Thames, A., González Abad, G., Ryerson, T. B., Thompson, C. R., Peischl, J., McKain, K., Sweeney, C., Wennberg, P. O., Kim, M., Crounse, J. D., Hall, S. R., Ullmann, K., Diskin, G., Bui, P., Chang, C., and Dean-Day, J.: Mapping hydroxyl variability throughout the global remote troposphere via synthesis of airborne and satellite formaldehyde observations, *P. Natl. Acad. Sci. USA*, 116, 11171–11180, 2019.
- World Bank: World Bank Indicators, <https://data.worldbank.org/indicator/NY.GDP.MKTP.KD.ZG?locations=QA> (last access: 25 October 2023), 2022.
- Yienger, J. and Levy, H.: Empirical model of global soil-biogenic NO_x emissions, *J. Geophys. Res.-Atmos.*, 100, 11447–11464, 1995.